Int. J. Therm. Sci. (2001) 40, 702–716

S1290-0729(01)01259-5/FLA

Numerical study of the unstable thermocapillary flow in a silicon float zone under μ–g condition

Hussein Bazzi [a], Cong Tam Nguyen [a*], Nicolas Galanis [b]

[a] *Faculty of Engineering, Université de Moncton, Moncton, New Brunswick, Canada E1A 3E9*

[b] *Department of Mechanical Engineering, Faculty of Engineering, Université de Sherbrooke, Sherbrooke (Québec), Canada J1K 2R1*

(Received 4 May 2000, accepted 29 September 2000)

Abstract — In this work, the problem of the hydrodynamic instabilities of the thermocapillary flow inside a Silicon ($Pr = 0.016$) float zone supported by a pair of coaxial disks and operating under μ–g conditions has been investigated. The system of the conservation equations corresponding to a three-dimensional transient model was directly solved by employing a finite control volumes method fully-implicit in time and a staggered spatial mesh in the cylindrical coordinates system. Results have shown that for a low Marangoni number or a low temperature difference between the disks, the flow remains steady and consists of a perfectly axisymmetrical toroidal structure with the vortex center located beneath the free surface near the cold disk. Beyond the first critical Marangoni number, say $Ma_{cr}^1 \approx 48$, the transition from the axisymmetrical to the steady three-dimensional state has been observed. The flow structure consists of a drastically distorted torus with its vortex centers displaced both radially and axially and is located along a 'saddle-like' curve. At the second critical Marangoni number, say $Ma_{cr}^2 \approx 80$, the transition from this three-dimensional-steady-state to the three-dimensional-oscillatory state occurs. Under the effects of some azimuthally travelling instabilities, the entire velocity and temperature fields rotate around the main axis; and a dependent variable varies periodically both in time and space. The flow instabilities, which appear similar to those of the theoretical 'unstable vortex ring', are believed to be of the hydrodynamic origin. A detailed description of the internal flow structure and its dynamic behavior as well as a comparison with the previous numerical and experimental data have been given.

instability / transition / thermocapillary flow convection / float zone / silicon / micro-gravity / numerical simulation

Nomenclature

A	aspect ratio $= R_0/H$	
C_p	specific heat of the fluid	$J{\cdot}kg^{-1}{\cdot}K^{-1}$
H	height of the float zone	m
k	thermal conductivity of the fluid	$W{\cdot}m^{-1}{\cdot}K^{-1}$
Ma	Marangoni number $= \lvert\partial\sigma/\partial T\rvert \Delta T H/\mu\alpha$	
Ma_{cr}^1	the first critical Marangoni number	
Ma_{cr}^2	the second critical Marangoni number	
P	dimensionless pressure	
Pr	Prandtl number $= C_p\mu/k$	
R, θ, Z	dimensionless radial, tangential and axial coordinates	
R_0	radius of the zone	m
t, T	dimensional and dimensionless temperature	K
t_M	melting temperature of the material	K
t_H	heated disk temperature on a step	K
t_2	cold disk temperature $= t_M$	K
V_R	dimensionless radial velocity component	
V_θ	dimensionless tangential velocity component	
V_Z	dimensionless axial velocity component	
ΔT	reference temperature difference $= t_H - t_2$	K
α	thermal diffusivity	$m^2{\cdot}s^{-1}$
γ	constant $\lvert\partial\sigma/\partial T\rvert$	$N{\cdot}m^{-1}{\cdot}K^{-1}$
μ	dynamic viscosity	$kg{\cdot}m^{-1}{\cdot}s^{-1}$
ρ	density	$kg{\cdot}m^{-3}$
σ	surface tension of liquid-vapor interface	$N{\cdot}m^{-1}$
τ	time	s
τ^*	dimensionless time	

* Correspondence and reprints.
E-mail address: nguyenc@umoncton.ca (C.T. Nguyen).

1. INTRODUCTION

The float zoning technique [1] has become one of the interesting means to produce highly homogeneous and large crystals in space. Despite of a reduced effects of the natural convection under the micro-gravity conditions, the presence of the thermocapillary convection flow may influence the entire domain. Its effects on the thermal field within a float zone have received a particular attention from researchers, both experimentally [2–7] and numerically [8–16]. An interested reader may consult a partial review of previous works published in [17]. Recent observations in Space as well as on Earth have shown that the steady axisymmetrical thermocapillary flow may become oscillatory and non-symmetrical when it becomes sufficiently vigorous. In fact, the oscillatory flow inside a $NaNO_3$ ($Pr \approx 8.9$) float zone of ≈ 6 mm in diameter and ≈ 4 mm in height has been observed [4]. Two different oscillatory modes were noticed: the first mode or the non-symmetrical mode detected for $R_0/H \leq 0.77$ and the second mode or the symmetrical mode for the range $1.43 \geq R_0/H \geq 0.71$. Several models of the instability mechanism have been proposed. Some researchers [3, 4] believed that the thermocapillary flow may become unstable (i.e., oscillatory) when the Marangoni number exceeds a certain critical value Ma_{cr}, say $Ma_{cr} \approx 10000$ (for $NaNO_3$). The value of Ma_{cr} remains likely constant for a given material in Space and on Earth and seems to be proportional to $Pr^{0.75}$. On the other hand, it has been shown that the flexibility of the free surface itself may constitute a major factor in the generation of the oscillations [18, 19]. An interesting physical model has been proposed [5] in which, the axisymmetrical/oscillatory transition may likely be caused by a delay in the time-response between the thermocapillary flow and the return one coming from the interior region. It has been suggested [20] that the existence of a very thin thermal boundary-layer beneath the free surface may be a possible cause of the oscillatory flow. The instability of the buoyant layers inside a float zone has also been studied [7]. On the other hand, it has been stipulated [21] that the oscillatory state may occur when the dynamic Weber number We_d—defined as the ratio of the dynamic pressure $\rho V^2/2$ and the rigidity due to the surface tension σ/H at the free surface—reaches a certain critical limit. They have proposed a new dimensionless parameter, namely $s = (2We_d)^{1/2}$ to characterize the onset of the oscillations.

The existence of such an oscillatory flow, which may induce some undesirable inhomogeneities—called 'striations'—in the microscopic structure of the crystals themselves [41], has raised numerous analytical and numerical studies from researchers. An oscillatory flow within a half-zone of several liquids has been first numerically simulated [22] where the agreement between their numerical results and experimental data can be qualified as quite acceptable, except for the oscillation frequencies. A full-zone of Silicon was also studied [8, 23, 24], considering a deformable free surface but conserving however the axis-symmetry character of the flow field. These authors have also investigated the oscillatory behavior of the flow. The problem of the Rayleigh–Marangoni instabilities in a vertical cylinder has been considered [25] by using a finite-volume technique and by introducing an ad-hoc axisymmetrical and three-dimensional disturbances in order to obtain bifurcation. In a recent study [26], the problem of the stability of the flow in a half-zone of a small Prandtl number fluid has been numerically investigated. The axisymmetrical thermocapillary flow has been found to be unstable to a steady non-axisymmetrical state for zone aspect ratio of 1. With further increase of the thermocapillary Reynolds number, the flow loses its stability to an oscillatory state. Recently, the oscillatory Marangoni convection in a Silicone-oil liquid bridge ($Pr = 30$ and $Pr = 74$) has been studied [27]. It has been suggested that immediately after the onset of the instability, the flow can be described by a standing wave and a pulsating temperature field. When the disturbances become large however, the tangential velocity causes the rotation of a 'temperature-spots' on the free surface so that the instability can be described by the dynamic model of an azimuthally traveling wave. In a more recent works [38, 39], the authors have thoroughly studied the oscillatory behaviors of the thermocapillary flow in a $NaNO_3$ half-zone under micro-gravity condition. The critical Marangoni number corresponding to the onset of the oscillations has been estimated to be 9750. The hysteresis phenomenon as well as the effects due to an increase of the heating ramp-rate have also been investigated.

In spite of these considerable efforts deployed to its regard, the physical mechanism that governs the onset of the time-dependent flow as well the comprehensive picture of the flow organization remain, unfortunately, not very well understood, especially for a very low Prandtl number fluid such as Silicon which is often used as a base material for an optical and electronic components.

In the present paper, the problem of the hydrodynamic instabilities of the Marangoni flow inside a cylindrical float zone has been investigated by direct numerical simulation of a full three-dimensional and time-dependent model, and this considering Silicon ($Pr = 0.016$) as the fluid. The flow and the thermal field were determined

and carefully scrutinized during their time-evolution following an imposed realistic heating scheme. The critical Marangoni numbers corresponding to the two successive transitions have been determined and the complete organization of the flow structure as well as the possible cause of the instability will be presented and discussed.

2. MATHEMATICAL MODELLING

2.1. Governing equations

We consider a cylindrical zone of a liquid suspended freely, under surface tension effects and micro-gravity condition, between a pair of coaxial and parallel disks, *figure 1*. The disks are held fixed at an uniform temperatures, respectively, t_1 and t_2, with $t_2 = t_M$ where t_M is the melting temperature of the material considered and $t_1 = f(\tau)$ varies as a known function of time. The fluid is considered to be Newtonian and incompressible with constant physical properties, except for the surface tension which is assumed to decrease linearly with the temperature:

$$\sigma = \sigma_M - \gamma(t - t_M) \tag{1}$$

where the constant γ is assumed to be positive meaning that the fluid particles will generally pull away from a high temperature region on the free surface. The viscous dissipation is considered negligible in the energy equation. The free surface of the zone is assumed thermally insulated and radially non-deformed, but can allow the transfer of heat and momentum in both the axial and circumferential directions. The condition of a thermally insulated surface represents quite appropriately the real situations often encountered in the experimental platforms. The assumption regarding the perfectly cylindrical shape of the free surface is motivated by the fact that for the cases considered, the capillary number, defined as $Ca = \gamma \Delta T/\sigma$, remains very small, say $Ca < 10^{-3}$, indicating the dominant effect of the surface tension force [38]. Furthermore, our numerical simulations considering the deformed free surface [28, 40] have clearly shown that, under micro-gravity condition (i.e., $\leq 10^{-4}$ g), the maximum radial deformation of the free surface did not exceed, in any case tested, 0.08% of the zone nominal radius.

In the present study, the following quantities H, $(\gamma \Delta T/\mu)$, $(H\mu/\gamma \Delta T)$, $\rho(\gamma \Delta T/\mu)^2$, and $\Delta T = t_H - t_M$ have been, respectively, adopted as the reference length, velocity, time, pressure and temperature difference (note that t_H is the hot disk temperature corresponding to the end of each of the heating steps considered, as shown in *figure 2*). A dimensionless variable is then obtained by normalizing the quantity considered with respect to the corresponding reference quantity, except for the dimensionless temperature which is defined as:

$$T = (t - t_2)/\Delta T \tag{2}$$

The dimensionless governing equations written in the cylindrical coordinates (R, θ, Z) system are as follows

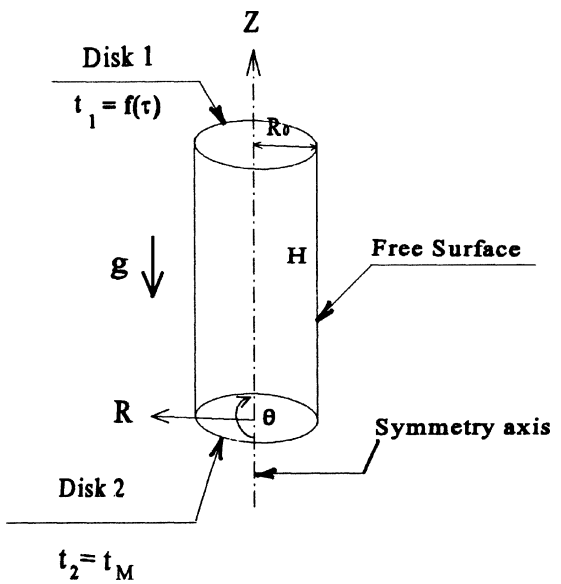

Figure 1. Geometry configuration of the problem under study.

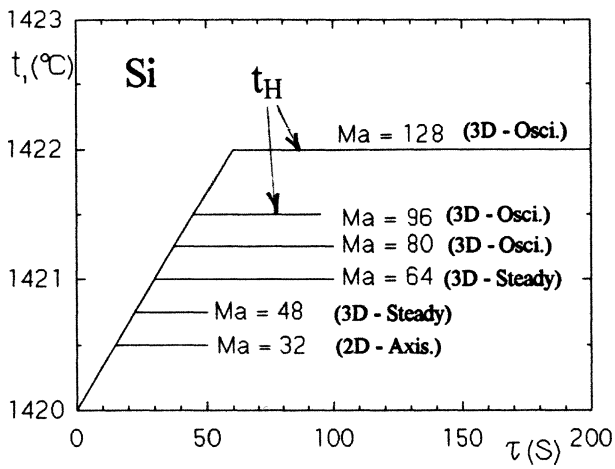

Figure 2. Time-variation of $t_1(\tau)$ as imposed for simulation of several cases with Silicon ($Pr = 0.016$, $A = 0.7$).

(see Bazzi [28]):

$$\nabla \cdot \mathbf{V} = 0 \tag{3}$$

$$\partial V_i/\partial \tau^* + \nabla \cdot (\mathbf{V} \cdot V_i) = -\nabla P + (Pr/Ma)\nabla^2 V_i + S_i, \quad i = 1, 2, 3 \tag{4}$$

$$\partial T/\partial \tau^* + \nabla \cdot (\mathbf{V} \cdot T) = (Pr/Ma)\nabla^2 T \tag{5}$$

where $\mathbf{V} = (V_\mathrm{R}, V_\theta, V_\mathrm{Z})$ is the velocity vector and S_1, S_2 and S_3 are the velocity-related stress terms given as follows:

– for $i = 1$, the radial direction:

$$S_1 = V_\theta V_\theta/R - (Pr/Ma) \times \left\{ V_\mathrm{R}/R^2 + \left(2/R^2\right)\partial V_\theta/\partial\theta \right\} \tag{6}$$

– for $i = 2$, the tangential direction:

$$S_2 = (Pr/Ma)\left\{ \left(2/R^2\right)\partial V_\mathrm{R}/\partial\theta - V_\theta/R^2 \right\} - V_\mathrm{R} V_\theta/R \tag{7}$$

– for $i = 3$, the axial direction:

$$S_3 = 0 \tag{8}$$

2.2. Boundary and initial conditions

The highly non-linear and coupled governing equations (3)–(5) must be appropriately solved subject to the following boundary and initial conditions:

– on both disks, the usual non-slip and non-penetration conditions prevail. The disk no. 2 is held at constant temperature $T_2 = 0$, while T_1 varies with time τ^* according to an *a priori* known function (shown in *figure 2*);

– the free surface, as stated previously, is considered thermally insulated and remains perfectly cylindrical. Also, the equilibrium of the shear stress in the axial and tangential directions along that surface must be fully satisfied. The resulting boundary conditions are then as follows:

at $R = A = R_0/H$:

$$V_\mathrm{R} = 0 \tag{9a}$$

$$\partial V_\mathrm{Z}/\partial R = -\partial T/\partial Z \tag{9b}$$

$$(1/A)\partial T/\partial\theta = -\{\partial V_\theta/\partial R - V_\theta/A\} \tag{9c}$$

$$\partial T/\partial R = 0 \tag{9d}$$

– *initial conditions*: we assume that at the beginning of the heating process, i.e., at $\tau^* = 0$, the quiescent condition applies with the fluid temperature equal to its melting temperature t_M throughout. In order to minimize any numerical error which may be accumulated during the search for the solution, these initial conditions have been systematically employed for each of the cases simulated.

The governing equations (3)–(5) and their boundary conditions reveal that the problem under consideration may be characterized by a set of three dimensionless parameters, namely the Marangoni number *Ma*, the Prandtl number *Pr* and the aspect ratio *A* (see the Nomenclature).

2.3. Numerical method and validation

The modified-SIMPLE method, which was successfully used in a previous study for a $NaNO_3$ float zone [38, 39], has been employed here again to solve the system of conservation equations (3)–(5) subject to the above boundary and initial conditions. Since this method has been very well documented elsewhere (see [29, 30]), only a brief review is given here. This method, as other member of the SIMPLE-codes family, is based on the finite control volume approach where each of the conservation equations is integrated over a finite volume using the exponential scheme for the treatment of the combined 'convection-and-diffusion' fluxes (of heat and momentum) resulting from the transport process, and the fully-implicit scheme for the transient term in the equations (4) and (5). Also, the staggered grids have been used where the velocity components are calculated at the center of the volume interfaces while the pressure as well as the other scalar quantities such as the temperature and the species concentration are computed at the center of the control-volume. The algebraic 'discretization equations' resulting from this integration process have been solved sequentially within each time step. A special 'pressure-correction' equation, which was obtained by combining the discretization form of the Navier–Stokes equations (4) and the one of the continuity equation (3), has been employed to compute the guessed pressure field as well as to correct the velocities field in order to satisfy progressively, i.e., in a iterative manner, all the discretization equations (see [29] for the complete details regarding the above numerical algorithm).

In order to ensure the consistency as well as the accuracy of the numerical results, several non-uniform grids have been submitted to an extensive testing procedure [38]. Results have show that the $26 \times 26 \times 24$ grid, respectively, 26, 26 and 24 control volumes in the radial, axial and tangential directions, with highly packed grid points along the domain boundaries—appears to be quite

satisfactory to ensure the precision of the numerical results. In conjunction with the high Marangoni numbers used in the test cases, the chosen grid appears to be quite appropriate for the entire range of the parameter *Ma* considered in this study [28, 38].

For all the numerical experiments performed in this work, a time step $\Delta\tau$ as small as $1/50$ s has been employed throughout. As convergence indicator at every time step, the so-called 'residual mass'—i.e., the residue resulting from the integration of the continuity equation (3) over a finite control-volumes—was systematically monitored and scrutinized. For all of the simulations performed, the maximum residual mass has been kept at a level as low as 0.001% (on the normalized basis).

The computer program has been extensively and successfully validated by comparing the calculated results with the available data in the literature for many cases. The quantitative comparison was carried out on the fluid axial velocity and temperature on the free surface, and this for both the steady and transient cases. In general, the agreement can be qualified as quite acceptable. The complete details regarding the study of the grid independence, the code validation as well as the other numerical information have been presented elsewhere (see [28, 38]).

3. THE HYDRODYNAMIC INSTABILITY OF A LOW PRANDTL NUMBER FLUID, Si

The fluid selected in this study is Silicon ($Pr = 0.016$) because of its wide application in various electronic components. During the numerical simulation of a typical case, the structure of the thermal and hydrodynamic fields has been carefully scrutinized while tracing through the increase of ΔT between the disks (or the Marangoni number). *Figure 2* shows the time-variation of the hot disk temperature as used for the simulated heating process. The flow nature corresponding to each of the levels of the parameter *Ma* considered has also been shown for discussion purpose. The heating ramp rate $\mathrm{d}t_1/\mathrm{d}\tau$ has been fixed to be $2\,^{\circ}\mathrm{C}\cdot\mathrm{min}^{-1}$, a value which appears to be experimentally realistic. Also, for each of the cases tested, a sufficiently large elapse-time has been allowed after having reached a constant level of ΔT in order to ascertain the nature, either steady or oscillatory, of the flow. The aspect ratio has been fixed to be 0.7 for all of the simulations performed for Si.

3.1. The flow basic state

For a relatively low value of *Ma*, say $Ma < 48$, it has been observed that the flow structure remains steady and perfectly axisymmetrical, *figure 3(a)*. It consists of an usual toroidal flow pattern with a strong fluid circulation observed in the vicinity of the free surface as well as in the central region of the liquid zone. Also, the vortex center is located near the free surface which is characteristic for any surface-tension-driving flow. It is interesting to observed that the vortex center is located on the side of the cold disk. Such a behavior, which seems to be proper to a low Prandtl number fluid, may be explained by the presence of high temperature gradient on the free surface near the cold disk, and as consequence, a high axial velocity prevails in that region [28, 40]. The steadiness of the flow is obvious from the *figure 3(b)* which shows identical temperature profiles for three particular points located on the free surface at the middle plane $Z = 0.5$. It has also been observed that the fluid circulation increases appreciably with the increase of the Marangoni number. Such a behavior is physically quite realistic and can be explained by the fact that increasing *Ma* corresponds directly to an increase of ΔT which, in turn, directly influences the driving-thermocapillary force on the free surface. Hence, in general, the fluid circulation within the zone will increase with the increase of *Ma*. The complete results regarding the structure as well as the behaviors of the flow and the temperature field corresponding to the axisymmetrical cases with Si have been presented in [28].

3.2. The first transition to the steady three-dimensional state

It is very interesting to observe that when the fluid circulation becomes vigorous enough, say for $80 > Ma \geq 48 \approx Ma^1_{\mathrm{cr}}$, the first transition from the above axisymmetrical state to the steady three-dimensional state occurs. The flow and the temperature field, although exhibiting clearly their three-dimensional character, remain however perfectly steady as confirmed from the temperature profiles obtained at three particular points located on the zone free surface, *figure 4* (these points are exactly those considered earlier in *figure 3(b)*). The internal flow structure is rather complex. *Figure 5* shows, for the case $Ma = 64$ for example, the corresponding isotherms, contours of V_Z as well as the structure of the transversal velocities in the cross-section at $Z = 0.5$. One can easily observe that the contours of the temperature and the axial velocity are no longer circular and concentric

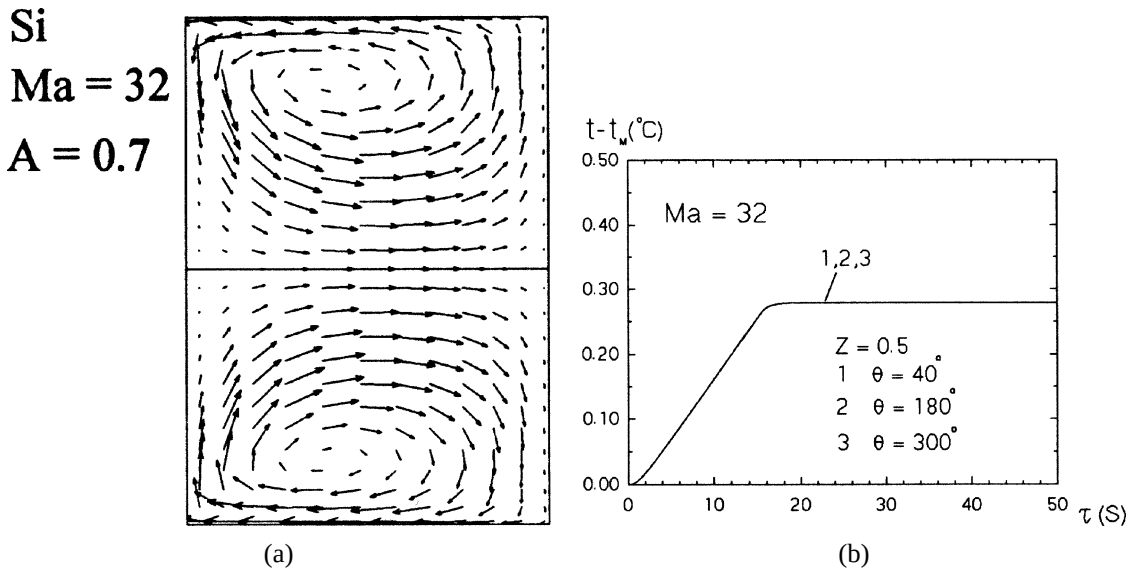

Figure 3. Basic state: the steady and axisymmetrical flow structure.

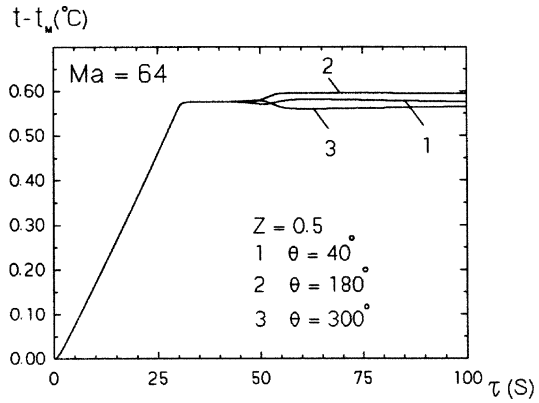

Figure 4. Onset of the transition from the steady-axisymmetrical to the steady-3D state ($Ma = 64$).

as in an axisymmetrical case, but are now distorted into an elongated elliptic shape, and they exhibit alternate regions of high and low gradients of T and V_Z along the circumference of the free surface. The elongated shape is similar for T and V_Z, i.e., a high temperature gradient region coincides with a low axial velocity gradient one, and vice-versa. From *figure 5(c)*, we can notice the presence of four different circulation zones which are symmetrical but counter-rotating by pair with respect to the center point. The strong secondary movement of the fluid directed against the free surface may be observed. It is very interesting to mention here that along the circumference of the free surface, the fluid pulls away from a cold region and directs toward an adjacent hot one which is, obviously, contrary to the well-known thermocapillary effect. This fact is very important since it indicates that the cause of the perturbations observed on the flow and temperature fields may be of the hydrodynamic origin, i.e., the instabilities appear to be first generated from some perturbations of the velocity field, as discussed later in Section 3.4. Another interesting consequence of this instability may also be observed on *figure 5(d)* which shows the structure of the isotherms on the free surface as obtained for the case $Ma = 64$ considered. Instead of the straight and parallel lines corresponding to the axisymmetrical case, the isotherms are now exhibiting clearly a 'wavy' pattern along the circumference, although the distortion observed does not appear visually to be very drastic. It is interesting to mention here that such a wavy pattern of the isotherms is similar to the one observed experimentally [34] on a $NaNO_3$ ($Pr = 8.9$) liquid zone (see also [38, 39]).

Figure 6(a)–(d) shows respectively, the structure of the velocity field as obtained in four different R–Z planes at $\theta = 0°$, 45°, 90° and 135° for the case $Ma = 64$. The radial and axial coordinates of the vortex center are also provided for discussion purpose. Since the flow appears to be diametrically symmetrical with respect to the singular point, i.e., the center of the cross-section, the reconstruction of the coherent structure of the flow may be then possible from *figure 6*. One can observe, at first, that the usual toroidal structure corresponding

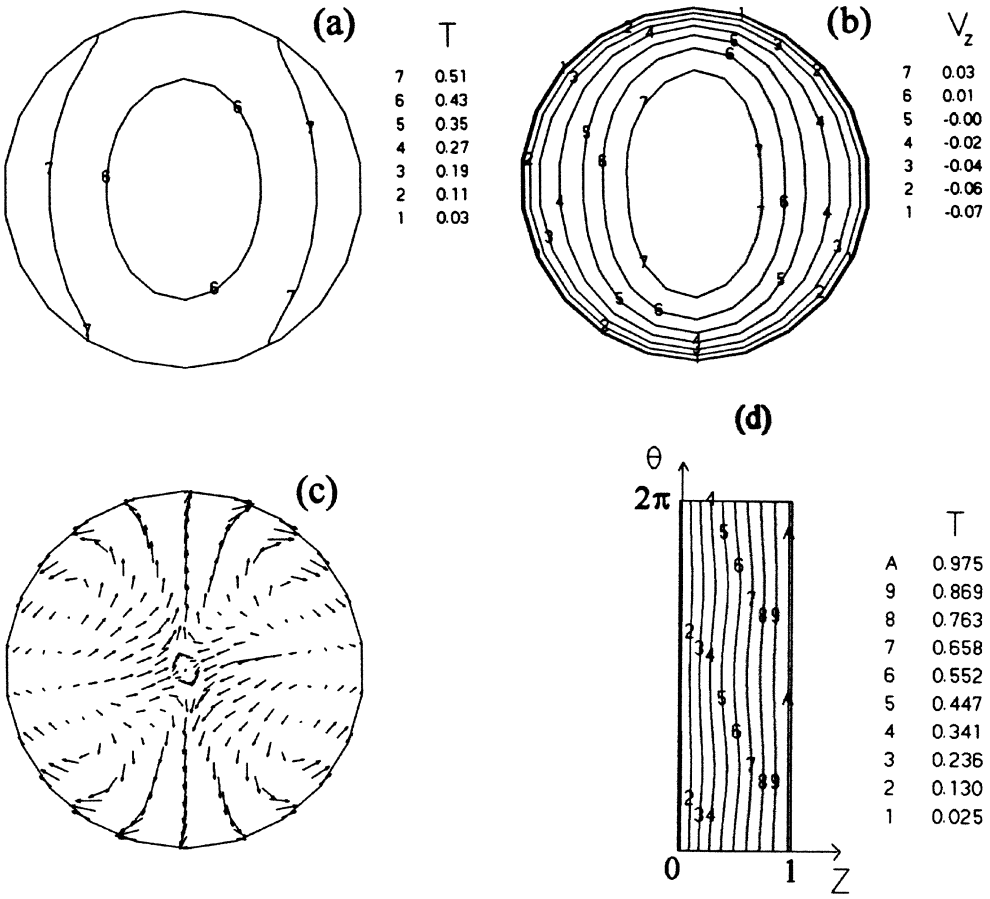

Figure 5. Steady and three-dimensional structure of isotherms (a), iso-contours of V_Z (b) and transversal velocities (c) in a middle cross-section; and structure of isotherms on the zone free surface (d), for the case $Ma = 64$.

to the thermocapillary basic flow still prevails, with a strong fluid circulation noticed beneath the free surface and the vortex center located near that surface. We note, however, that the location of this vortex center as well as the entire velocity field in the bulk fluid region change considerably from one R–Z plane to another. The shift in the position of the vortex center appears to be very important, particularly along the axial direction where its coordinate has shift from $Z = 0.5$ at $\theta = 0°$ to $Z = 0.41$ at $\theta = 45°$, and to its extreme position, $Z = 0.26$ at $\theta = 90°$ and finally to $Z = 0.39$ at $\theta = 135°$. In fact, for the case under consideration, the vortex center follows an elongated elliptic path in the R–θ plane. Thus, the steady pathway of the vortex center would take the form of a 'saddle–shape' (similar to the one shown later in *figure 12(b)*). The velocity field has also changed drastically, see, for example, *figures 6 (a)* and *(c)* for the corresponding extreme positions of the vortex center. In summary, after the first transition point corresponding to $Ma = Ma^1_{cr} \approx 48$, although the primary toroidal flow structure does still exist, the latter is subjected to a severe distortion under the effects of the hydrodynamic instability.

3.3. The second transition to the three-dimensional oscillatory state

With further increase of the temperature difference between the disks or the Marangoni number, say for $Ma \geq Ma^2_{cr} \approx 80$, the second transition from the above 3D-steady state to the 3D-oscillatory state clearly occurs. The latter is characterizing by a periodic time-variation of a dependent variable with respect to the time at a fixed point in space, but the perturbations have been found to be space-dependent as well. *Figure 7* shows eloquently, for the case $Ma = 128$ in particular, such periodicity in time at three particular points located on the free

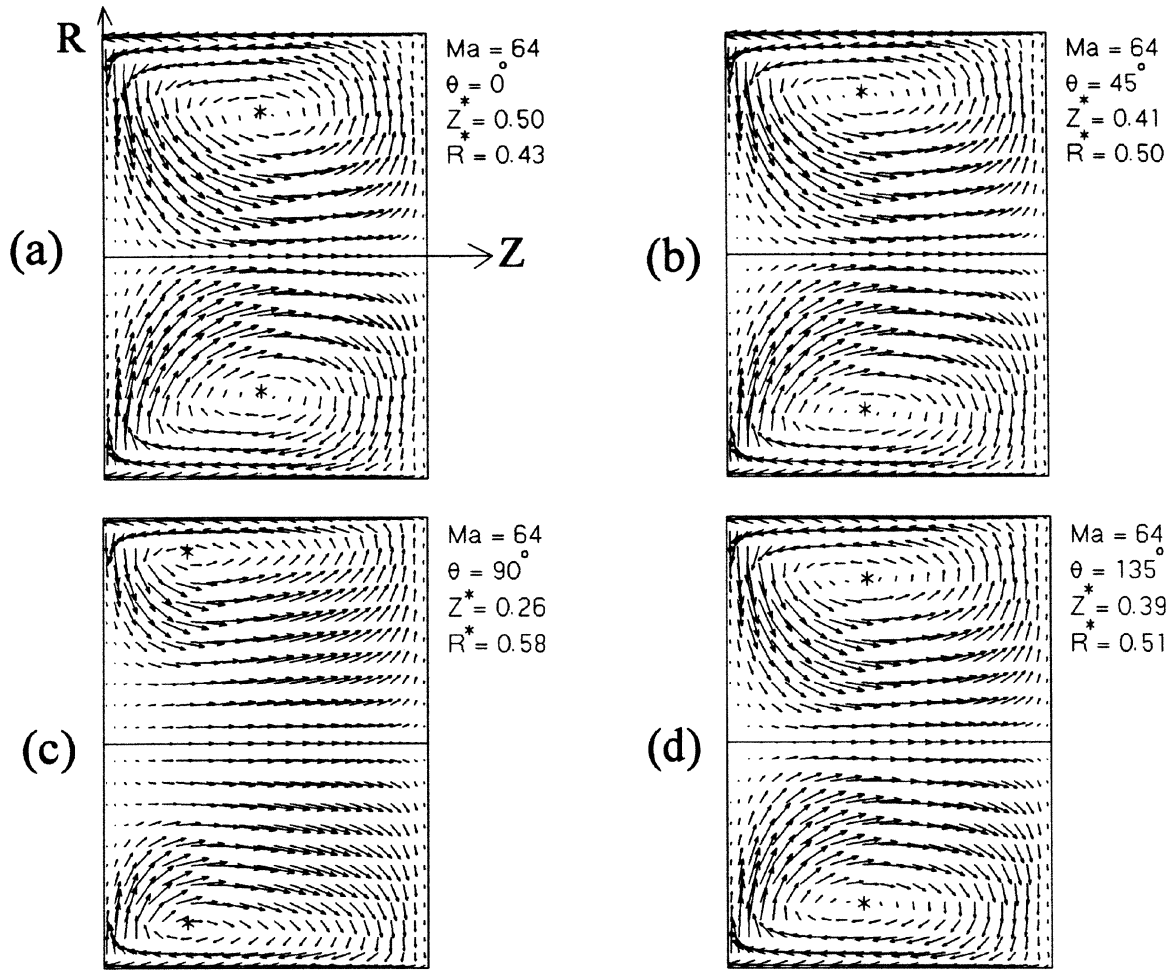

Figure 6. Steady-three-dimensional flow structure in four different R-Z planes ($Ma = 64$).

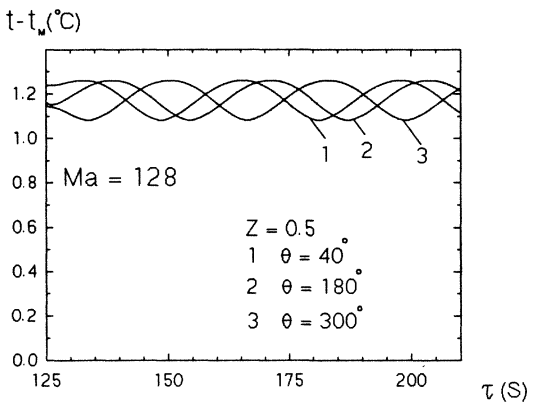

Figure 7. Temperature oscillations for three particular points on the free surface ($Ma = 128$).

surface (exactly the same points considered earlier in *figures 3(b)* and *4*). The peak-to-peak amplitude of the temperature oscillations is estimated to be 0.18 °C while the frequency has been determined to be 0.026 Hz by using a standard FFT technique. Such an oscillatory behavior can be better understood by scrutinizing the structure of the thermal field and its time-evolution. *Figures 8* and *9* show, respectively, for the case under consideration and for four different times during one complete cycle of the oscillations, the isotherms structure at the middle cross-section (at $Z = 0.5$) as well as those on the zone free surface. As observed before with the 3D-steady case (see again, *figure 5*), we can see that the similar effects due to the instability on the thermal field are also prevailing in the 3D-oscillatory case here. Thus, isotherms in a cross-section become drastically

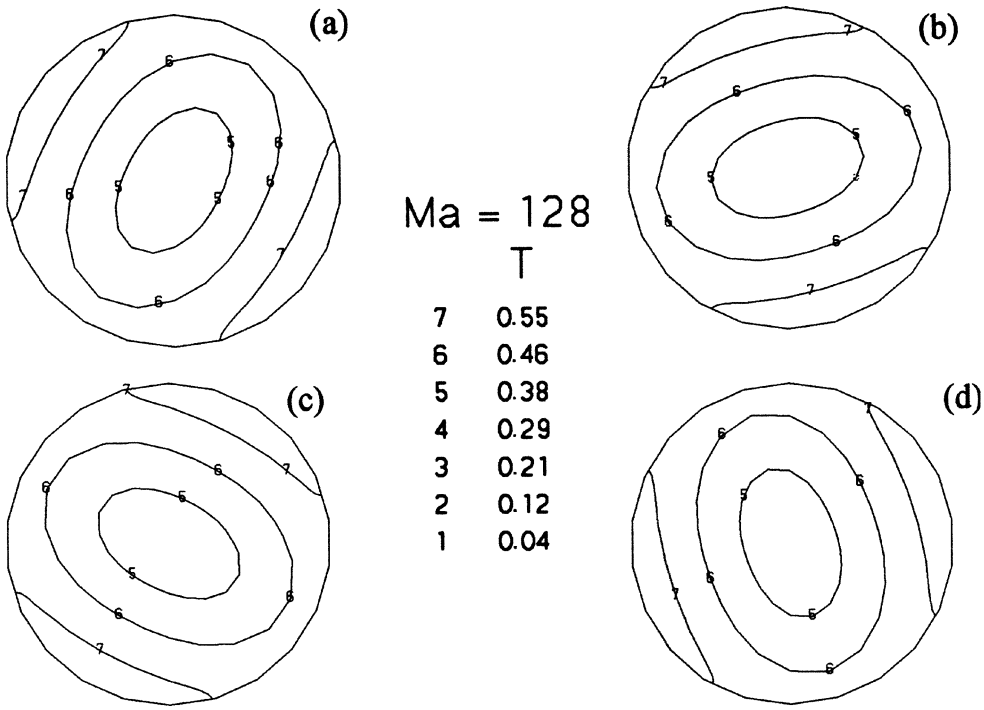

Figure 8. Instantaneous snapshot of the isotherms structure in a middle cross-section during one complete cycle of oscillation ($Ma = 128$).

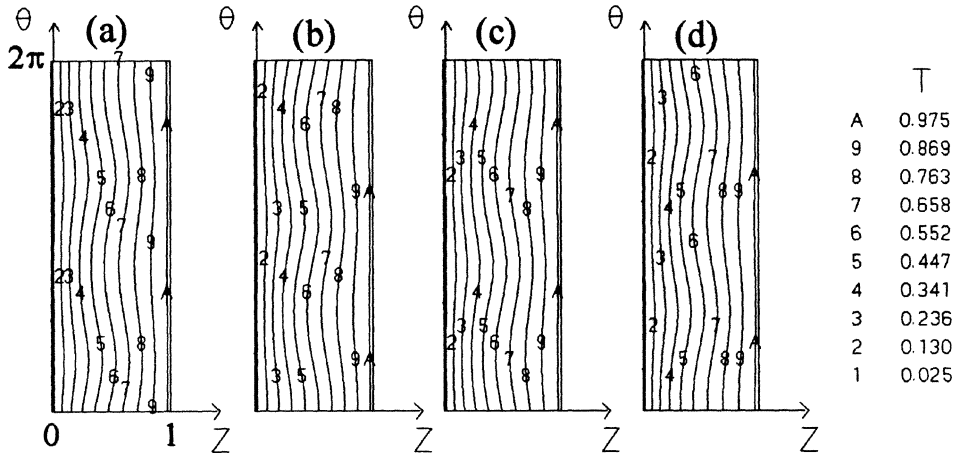

Figure 9. Instantaneous snapshot of the isotherms structure on the free surface during one complete cycle of oscillation ($Ma = 128$).

distorted into an elliptic shape where an alternate hot and cold zones do exist on the zone free surface. It is very interesting to observe that these distorted isotherms are not steady, but rotate in fact around the main axis while conserving their elliptic shape. Such a striking behavior creates, for a particular location, an oscillatory time-evolution of a dependent variable, for example the temperature, as seen previously on *figure 7*. These effects are believed to be due to some azimuthally traveling instabilities, as explained later in the Section 3.4. The effects due to these traveling instabilities have also been clearly noticed through the 'wavy' pattern of the isotherms on the free surface, *figure 9*. One can observe that for the case $Ma = 128$ under consideration here, the

distortion induced on the isotherms appears obviously more pronounced with respect to that of the earlier 3D-steady case $Ma = 64$ (see *figure 5(d)*), thus indicating that the instability effects are stronger with the increase of the Marangoni number. In fact, for the same points located at $Z = 0.5$ on the free surface which were considered previously in *figures 3(b)*, *4* and *7*, the peak-to-peak amplitude of the temperature oscillations has been determined to be 0.07 °C, 0.10 °C and 0.18 °C respectively for $Ma = 80$, 96 and 128. The flow under high Marangoni number appears to be more vulnerable to a disturbance. Such a behavior, which is consistent with the experimental observations (see, in particular [4]) as well as with the numerical predictions (see, for example, [27, 38]), may be explained by the fact that for a higher Marangoni number, the intensity of the thermocapillary flow increases considerably and hence, the destabilizing effect due to a vigorous convection would take over the beneficial stabilizing effect due to the fluid viscosity.

Figures 10 and *11* show respectively for the case $Ma = 128$ considered, the structure of the velocity field in the cross-section at $Z = 0.5$ for four different times during one cycle, as well as the instantaneous view of this velocity field at four different R–Z planes corresponding to $\theta = 0°$, 45°, 90° and 135°. Here again, as we have seen before with the 3D-steady case, the internal structure of the flow field in a R–θ plane is rather complex because of the existence of four different circulation zones within the bulk fluid region. The alternate areas where strong merging currents are directed radially outwards against the free surface may be clearly noticed; while in the adjacent areas, the collision of two counter-currents on the free surface results in a drastically reduced circulation of the fluid in a transversal plane. In general, the circumferential circulation of the fluid is more pronounced in the vicinity of the free surface than in the central core region. Also, it has been observed that the above complex flow structure exhibits clearly its 'rotating' behavior azimuthally around the circumference: the same transversal flow structure appears to move circumferentially in the clock-wise direction to another angular position and ultimately, will complete a full rotation after one period of oscillation. Another point of fundamental interest resides in the fact that the surface currents of the fluid on the free surface pull away from a cold region and direct towards another adjacent hot region (see *figures 8* and *10*). Such a striking behavior, as observed and discussed previously, indicates that the perturbations would be of the

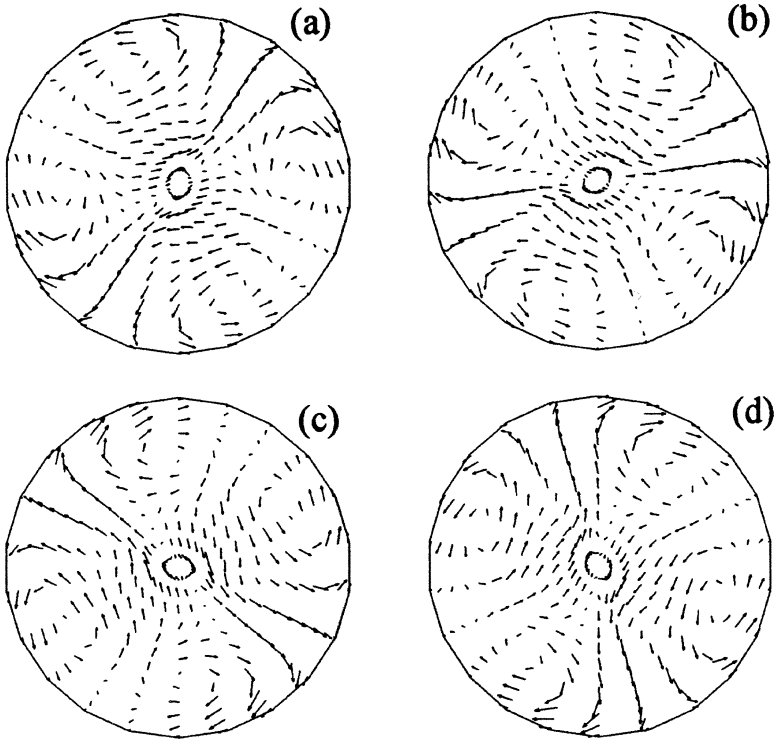

Figure 10. Instantaneous snapshot of the transversal flow structure in the middle cross-section during one complete cycle ($Ma = 128$).

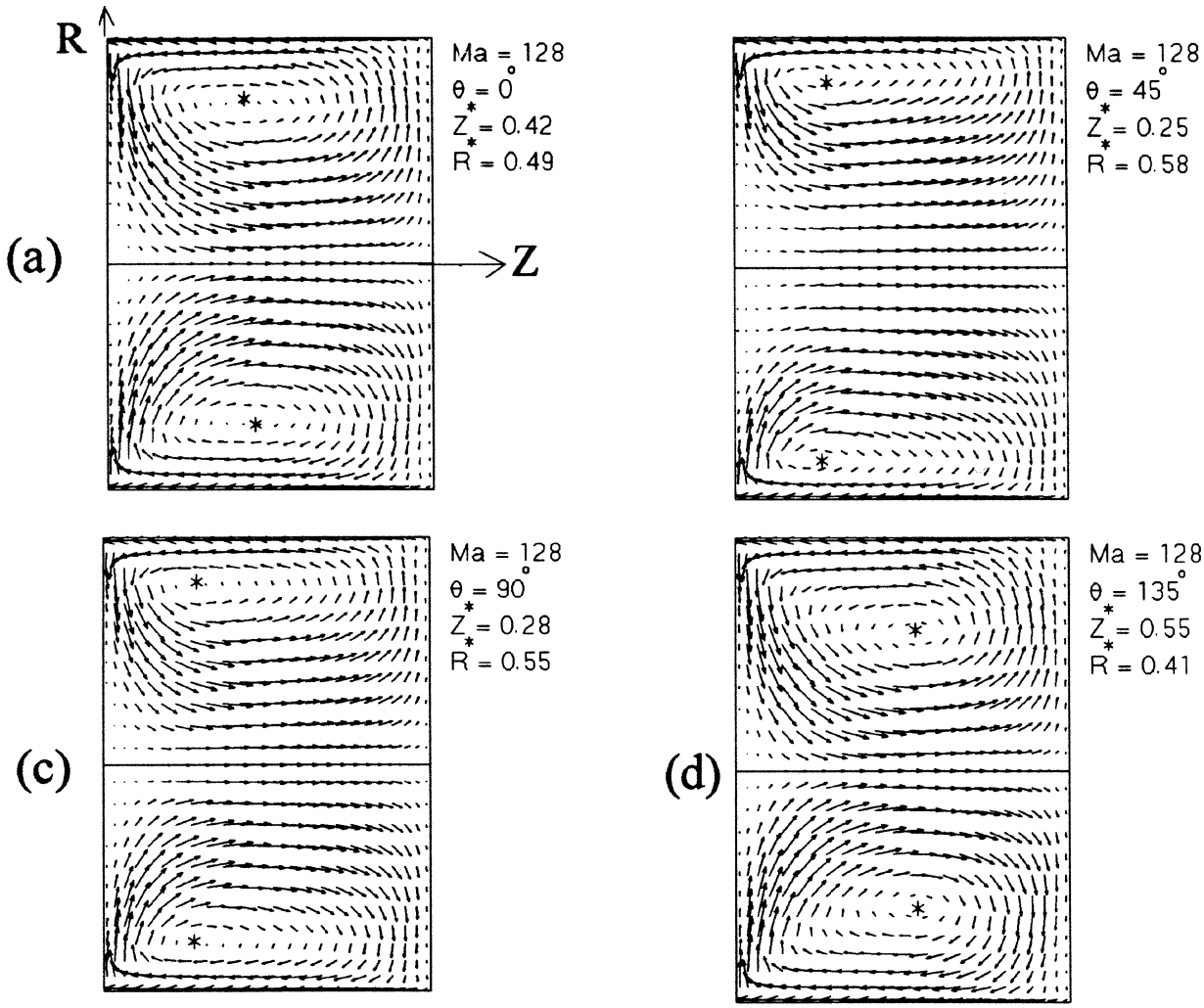

Figure 11. Instantaneous view of the flow structure in four different R–Z planes ($Ma = 128$).

hydrodynamic nature. In the same idea, it is interesting to mention here that for a moderate Prandtl number fluid such as $NaNO_3$ ($Pr = 8.9$), the flow instabilities appear to be of the thermal origin [38], i.e., they are first generated from some perturbations on the temperature field. With regard to the corresponding velocity field in a R–Z plane, the instantaneous snapshot for four different angular positions shows eloquently the drastic effects due to the instabilities on the flow structure, *figure 11*. One can clearly observe that under such effects, the entire velocity field is changing considerably from one angular position to another. The shift of the vortex center along both the radial and axial directions appears to be considerably pronounced at such a high Marangoni number considered here, say $Ma = 128$. Thus, the extreme positions of this vortex center may be detected at ($Z^* = 0.25$, $R^* = 0.58$) for $\theta = 45°$ and at ($Z^* = 0.55$, $R^* = 0.41$) for $\theta = 135°$. It is important to recall here that information displayed in *figure 11* are in fact instantaneous, i.e., taken at a given fixed time. As mentioned before, the entire velocity and temperature fields rotate around the main axis of the zone under the effect of an azimuthally traveling instabilities. Such a strikingly dynamical behavior, in particular for the vortex center, is shown in *figure 12* where the projected elliptic pathway of the vortex center is illustrated for two instants, say at τ and $\tau + \tau_0/2$(τ_0 is the oscillations period, estimated to be ≈ 38.46 s). In fact, for this case $Ma = 128$ or all other cases where the oscillatory

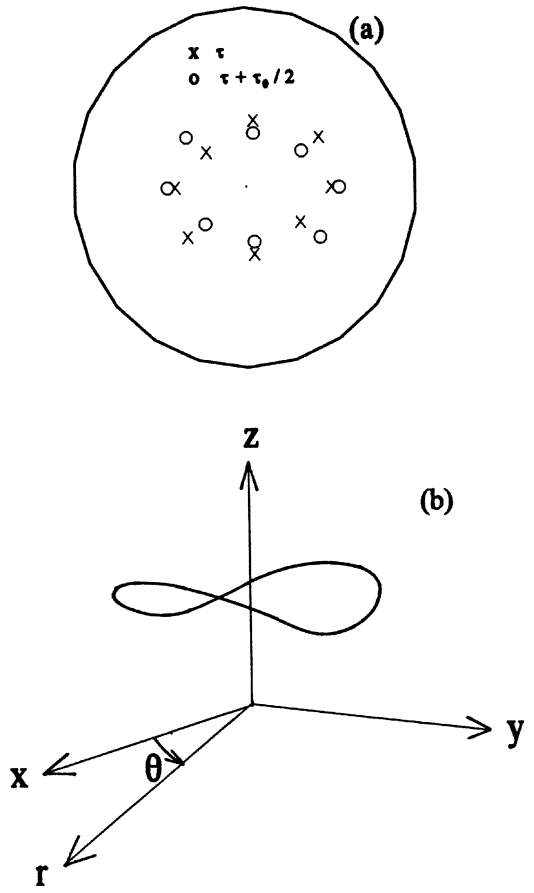

Figure 12. (a) Instantaneous positions of the vortex center in a R-θ plane for τ and $\tau + \tau_0/2$; (b) Instantaneous view of the pathway of the vortex center (not to scale).

state exists, the three-dimensional instantaneous view of the pathway of the vortex center looks like a 'saddle-like' shape as shown in *figure 12(b)*. Finally, for the same reason mentioned earlier regarding the vulnerability of the flow to a perturbation at high Marangoni number, it has been observed that the shift in the position of the vortex center appears to be more pronounced, although only slightly, with the increase of the parameter *Ma*.

3.4. On the possible cause of the instabilities

From the results shown previously, one can see that for a low value of the governing parameter *Ma*, say $Ma < 48$, the flow remains steady and perfectly axisymmetrical. Beyond the first critical Marangoni number, say $Ma^1_{cr} \approx 48$, the flow clearly exhibits its three-dimensional character but still remains steady. It is observed that, under the effects of some perturbations, the axial fluid circulation on the free surface is subject to a remarked circumferential deviation which is contrary with respect to the well-known thermocapillary law. With further increase of the forcing parameter Ma beyond the second critical Marangoni number, say $Ma^2_{cr} \approx 80$, the flow becomes oscillatory and exhibits clearly its 'rotating' character around the main axis. It is believed that both the 'steady' perturbations observed for $Ma^1_{cr} \leq Ma < Ma^2_{cr}$ as well as the 'dynamic' ones noticed for $\mathrm{Ma} \geqslant Ma^2_{cr}$ are the effects of a certain form of the flow instability. Thus, the thermocapillary effects appear to act only as the driving force in order to maintain the basic flow state (see again, *figure 3*) while the instability effects, once superimposed on this basic state, have created a striking three-dimensional flow organization observed previously. Such an instability has also been believed to be of the hydrodynamic nature, in conjunction with the earlier discussion regarding the anti-thermocapillary circulation of the fluid observed on the zone free surface.

It is very interesting to note here that the distorted torus as illustrated in *figures 11* and *12* seems to possess several common features with the one obtained from the theoretical 'unstable thin vortex ring' theory [36]. This study, based on the theory of the linear perturbations, has shown that a thin vortex ring of constant vorticity appears to be almost always unstable due to some local distortion that a single vortex filament may induce on itself. Such a behavior may exist as well inside a float zone where a vortex filament is, in fact, circumferentially continued and bounded. It should be noted that in the case of a cylindrical float zone as the one under study here, the presence of the disks rends somewhat difficult any direct comparison, in spite of the close similarity between the two problems considered. From the above unstable 'thin vortex ring' theory, it has been established that after the onset of the instabilities, the vortex center would shift in a sinusoidal manner along the torus perimeter, vertically as well as radially, on a lines inclined at 45° with respect to the vertical main axis. Due to this inclination, a part of the torus is moving towards the center while going downward, and the other part of the torus is shifting upwards while approaching the center. In the case considered here, although some displacement of the vortex center is clearly noticed, its movement seems not to obey exactly to the above description, probably due to the presence of the solid disks. It has been believed that the instability form similar to that of an unstable vortex ring may be the possible cause of the perturbations observed so far in this work on the Silicon float zone. Such an instability may produce, as results, a non-zero circumferential velocity of the fluid.

It has been noticed, numerically, that immediately after the first transition point, this circumferential velocity remains very weak so that perturbations on the flow field appear to be 'steady' with respect to the θ-direction (see again, *figures 5* and *6*). But with a further increase of the forcing parameter *Ma*, the instability grows considerably inside the zone which results in a more pronounced displacement of the vortex center and a higher tangential velocity component. Hence, the 'rotating' effect would set in creating a striking effects as observed before (see again, *figures 8, 9* and *10*).

3.5. Comparison with other experimental and numerical data

Due to the fact that Silicon is a non-transparent fluid, there were practically no direct observations on the internal flow structure. The oscillatory behaviors of a Silicon float zone was first studied experimentally in [37]. It has been found that the second critical Marangoni number Ma^2_{cr} (the one corresponding to the onset of the oscillations) likely lies within the interval 61–87. However, the first critical Marangoni number Ma^1_{cr} (the one which corresponds to the onset of the 3D-steady-state) has not yet been measured experimentally. *Table I* shows the limited comparison between our values as obtained for Ma^1_{cr} and Ma^2_{cr} with other numerical and experimental data. The agreement with the experimental data for Si from [37] as well as with the numerical results from [26] (for fluid with $Pr = 0.01$) can be qualified as quite acceptable. Our value predicted for Ma^2_{cr} is also close to the one calculated by using $Pr = 0.016$ and the empirical correlation proposed in [42] for various low Prandtl number fluids. With regard to the numerical work published in [23, 24], there was no possible comparison due mainly to the 2D-axisymmetrical assumption adopted in this work. Such an assumption has eliminated virtually all possibility to obtain numerically a real three-dimensional flow.

TABLE I
Comparison with other experimental and numerical data.

	(1)	(2, 3)	(4)	(5)
Ma^1_{cr}	48	–	19.6	–
Ma^2_{cr}	80	$\approx$ 61–87 (2) 93.7 (3)	62.5	200

(1) Numerical results $Pr = 0.016$, this work.
(2) Experimental data from [37] for Silicon.
(3) Empirical correlation from [42] with $Pr = 0.016$.
(4) Numerical results from [26] for $Pr = 0.01$.
(5) Numerical results from [22] for $Pr = 0.02$.

Finally, it should be noted that the critical Marangoni number increases with the Prandtl number, because of the augmentation in the stabilizing effects due to the fluid viscosity. Therefore, it is somewhat expected that our value as obtained for Ma^2_{cr} would fall between the value predicted by [26] and the one by [22]. Such a dependence of Ma^2_{cr} on the fluid Prandtl number appears to be quite consistent with that observed experimentally (see, for example, [42]).

4. CONCLUSION

In this paper, we have investigated, by direct numerical simulation, the transient behaviors of the flow inside a cylindrical Silicon float zone under μ–g condition. The conservation equations resulted from a full 3-D and time-dependent model have been solved by employing the modified-SIMPLE method. Results have clearly shown that for a low Marangoni number, say $Ma < 48$, the flow remains steady and perfectly axisymmetrical. For the intermediate range of *Ma*, say $Ma^1_{cr} \approx 48 \leq Ma < 80$, the transition from this steady-axisymmetrical to the steady-3D state occurs. The toroidal flow structure exhibits a drastic distortion due to the radial and axial shift of the vortex center from one angular position to another. With a further increase of the Marangoni number beyond the second critical Marangoni number, say $Ma^2_{cr} \approx 80$, the second transition from this steady-3D state to the oscillatory-3D state occurs. Under the effects of the azimuthally traveling instability, the entire flow and thermal fields rotate around the zone main axis. On the free surface, the fluid is subjected to a pronounced and anti-thermocapillary deviations along the circumference. The vortex center exhibits a drastic shift along the 'saddle-like' curve which is both time and space-dependent. The instabilities, which result in the two transitions, are believed to be of the hydrodynamic origin and similar to those of the theoretical 'unstable thin vortex ring'.

Acknowledgements

The authors wish to thank the Natural Sciences and Engineering Research Council of Canada, the Ministry of Intergovernmental and Aboriginal Affairs of New Brunswick, the "Ministère de l'Éducation du Québec" and the Faculty of the Graduate Studies and Research of the "Université de Moncton" for financial support to this project. Thanks are also due to the Faculty of Engineering of the "Université de Moncton" for allocating the computing facilities.

REFERENCES

[1] Pfann W.G., Zone Melting, 2nd ed., Wiely, New York, 1966.

[2] Schwabe D., Sharmann A., Some evidence for the existence and a magnitude of a critical Marangoni number for the onset of oscillatory flow in crystal growth melts, J. Crystal Growth 46 (1979) 125–131.

[3] Chun Ch.H., Marangoni convection in a floating zone under reduced gravity, J. Crystal Growth 48 (1980) 600–610.

[4] Preisser F., Schwabe D., Sharmann A., Steady and oscillatory thermocapillary convection in liquid columns with free cylindrical surface, J. Fluid Mech. 126 (1983) 545–567.

[5] Ostrach S., Kamotani Y., Lai C.L., Oscillatory thermocapillary flows, Physico-Chemical Hydrodynamics 6 (1985) 585–599.

[6] Monti R., Fortezza R., The scientific results of the experiment on oscillatory Marangoni flow performed in telescience on texus 23, Micrograv. Q. 1 (1991) 163.

[7] Hu W.R., The influence of buoyancy on the oscillatory thermocapillary convection with small Bond number, 39th IAF Congress, Paper No. IAF-88-365, 1988.

[8] Kazarinoff N.D., Wilkowski J.S., A numerical study of Marangoni flows in zone-refined Silicon crystals, Phys. Fluids A 1 (1989) 625–627.

[9] Clark P.A., Wilcox W.R., Influence of gravity on thermocapillary convection in floating zone melting of Silicon, J. Cryst. Growth 50 (1980) 461.

[10] Xu J.J., Davis S.H., Liquid bridges with thermocapillarities, Phys. Fluids 26 (1983) 2880–2886.

[11] Rybicki A., Florian J.M., Thermocapillary effects in liquid bridges. I. Thermocapillary convection, Phys. Fluids 30 (1987) 1956.

[12] Rybicki A., Florian J.M., Thermocapillary effects in liquid bridges. II. Deformation of the interface and capillary instability, Phys. Fluids 30 (1987) 1973.

[13] Chen G., Roux B., An analytical study of thermocapillary flow and surface deformation in floating zones, Micrograv. Q. 1 (1991) 73.

[14] Napolitano L.G., Viviani A., Marangoni–Stokes flow in axisymmetric bridges, Micrograv. Q. 2 (1992) 179.

[15] Chen H., Saghir M.Z., Three-dimensional Marangoni convection in the asymmetrically heated float zone, Micrograv. Q. 4 (1994) 39.

[16] Bazzi H., Nguyen C.T., Galanis N., Transient behaviors of a $NaNO_3$ float zone operating under high Marangoni number condition, in: Proc. 1997 ASME Fluids Engineering Division—Summer Meeting, Vancouver (B.C.), Canada, 1997, Paper No. FEDSM-3390.

[17] Wilcox W.R., Floating zone melting of electronic materials in space, in: Proc. 29th AIAA Conf., 1991, Paper no. AIAA-91-0507.

[18] Vargas M., Ostrach S., Kamotani Y., Surface tension driven convection in simulated floating zone configuration, Report, Case Western Reserve University, 1982.

[19] Kamotani Y., Ostrach S., Vargas M., Oscillatory thermocapillary convection in a simulated floating zone configuration, J. Crystal Growth 66 (1984) 83–90.

[20] Kamotani Y., Lee K.J., Oscillatory thermocapillary flow in a liquid column heated by a ring heater, Physico-Chemical Hydrodynamics 11 (1989) 729–736.

[21] Napolitano L.G., Monti R., Surface driven flows: recent theoretical and experimental results, ESA SP 256 (1987) 551–555.

[22] Rupp R., Müller G., Neumann G., Three-dimensional time-dependent modeling of the Marangoni convection in zone melting configuration of GaAs, J. Crystal Growth 97 (1) (1989) 34–41.

[23] Kazarinoff N.D., Wilkowski J.S., Marangoni flows in a cylindrical liquid bridge of Silicon, in: Roux B. (Ed.), Numerical Simulation of Oscillatory Convection in Low Pr Fluids, Vieweg, Braunschweig, 1990, pp. 65–73.

[24] Kazarinoff N.D., Wilkowski J.S., Period tripling and subharmonic oscillations in Marangoni flows in a cylindrical liquid bridge, in: Wong R. (Ed.), Proc. Int. Symp. On Asymptotic Comput. Anal., Lecture Notes in Pure Appl. Math., Vol. 24, Dekker, New York, 1990, pp. 265–283.

[25] Wagner C., Friedrich R., Comments on the numerical investigation of Rayleigh and Marangoni convection in a vertical circular cylinder, Phys. Fluids 6 (1994) 1425.

[26] Levenstam M., Amberg G., Hydrodynamical instabilities of thermocapillary flow in a half-zone, J. Fluid Mech. 297 (1995) 357–372.

[27] Savino R., Monti R., Oscillatory Marangoni convection in cylindrical liquid bridges, Phys. Fluids 8 (11) (1996) 2906–2922.

[28] Bazzi H., Transient behaviors of Float Zones under 1-g and μ-g Environments—the Laminar–Oscillatory-Transition "Etude numérique de l'écoulement transitoire dans une zone flottante—La transition axisymétrique/oscillatoire", Ph.D. thesis, Department of Mechanical Engineering, Université de Sherbrooke, Québec, Canada, 1999, 239 p.

[29] Patankar S.V., Numerical Heat Transfer and Fluid Flow, Hemisphere, Washington, DC, 1980.

[30] Innovative Research Inc. microCOMPACT V. 4.0, Reference Manual, Maple Grove, Minnesota (USA), 1996.

[31] Bazzi H., Nguyen C.T., Galanis N., Oscillatory thermocapillary flow in Silicon float zone under μ-g condition, in: Proceedings of 11 IHTC, Vol. 4, 1998, pp. 429–434.

[32] Okano Y., Hatano A., Hirata A., Natural and Marangoni convection in a floating zones, J. Chem. Engrg. Japan 22 (4) (1989) 385–388.

[33] Saghir M.Z., Rosenblat S., Numerical simulation of tetracosane and cadmium mercury telleride in 1-g and 10^{-3} g environment, in: Proc. 7th European Symp. On Material and Fluid Sciences in Microgravity, ESA SP-295, 1990.

[34] Schwabe D., Scharmann A., Measurements of the critical Marangoni number of the laminar-oscillatory transition of thermocapillary convection in floating zones, in: Proc. 5th European Symp. On Material and Fluid Sciences in Microgravity, ESA SP-222, 1984, pp. 281–289.

[35] Schwabe D., Scharmann A., Measurement of the critical Marangoni number in a floating zone under reduced gravity, in: Proc. 4th European Symp. On Material and Fluid Sciences in Microgravity, ESA SP-191, 1983, pp. 213–218.

[36] Widnall, Tsai, The instability of the thin vortex ring of constant vorticity, in: Proceeding. R. Soc. Londres A287, 1977.

[37] Cröll A., Müller-Sebert W., Nitsche R., The critical Marangoni number for the onset of time-dependent convection in Silicone, Materials Res. Bull 24 (1989) 995–1004.

[38] Bazzi H., Nguyen C.T., Galanis N., Numerical simulation of oscillatory Marangoni convective flow inside a cylindrical liquid zone, Internat. J. Therm. Sci. 38 (1999) 863–878.

[39] Nguyen C.T., Bazzi H., Galanis N., Unstable thermocapillary flow inside a $NaNO_3$ float zone, in: Proc. 6th International Conference On Advanced Computational Methods in Heat Transfer, Madrid (Spain), 2000, pp. 31–41.

[40] Bazzi H., Nguyen C.T., Galanis N., Transient behaviours of float zones in μ–g and 1–g environments, in: Lewis R.W. (Ed.), Internat. J. Numer. Meth. Heat Fluid Flow 10 (3) (2000) 307–333.

[41] Brown R.A., Theory of transport process in single crystal growth from the melt, A. I. Chem. E. J. 34 (6) (1988) 881–911.

[42] Cröll A., Kaiser Th., Schweiser M., Danilewsky A.N., Lauer S., Tegetmeier A., Benz K.W., Floating-zone and floating-solution-zone growth of GaSb under microgravity, J. Crystal Growth 191 (1998) 365–376.